RESEARCH ARTICLE | APRIL 09 2026

Verification of kinetic model for liquid molecule transport within adsorption layers on solid surfaces via molecular dynamics simulation

Naohiro Dezawa; Donatas Surblys ; Gota Kikugawa ; Takeo Nakano ; Taku Ohara

J. Chem. Phys. 164, 144305 (2026)
https://doi.org/10.1063/5.0331495

The Journal of Chemical Physics ARTICLE pubs.aip.org/aip/jcp

Verification of kinetic model for liquid molecule transport within adsorption layers on solid surfaces via molecular dynamics simulation

Cite as: J. Chem. Phys. 164, 144305 (2026); doi: 10.1063/5.0331495
Submitted: 25 February 2026 • Accepted: 17 March 2026 •
Published Online: 9 April 2026

Naohiro Dezawa,[1,2] Donatas Surblys,[1,a)] Gota Kikugawa,[1] Takeo Nakano,[3] and Taku Ohara[1]

AFFILIATIONS

[1] Tohoku University Institute of Fluid Science, 2-1-1 Katahira, Aoba-ku, Sendai 980-8577, Japan
[2] Department of Finemechanics, Graduate School of Engineering, Tohoku University, 6-6 Aramaki-Aoba, Aoba-ku, Sendai 980-0845, Japan
[3] Tokyo Electron Technology Solutions Ltd., 650 Mitsuzawa, Hosaka-cho, Nirasaki 407-0192, Japan

[a)] **Author to whom correspondence should be addressed:** donatas@tohoku.ac.jp

ABSTRACT

In the manufacturing process of semiconductor devices, wet processes such as cleaning and chemical treatment on surfaces with nanoscale fine structures play a critical role. The mass transport within nanoscale structures exhibits properties different from those of bulk liquids, owing to the influence of layered adsorption structures of liquid molecules formed near solid–liquid interfaces. In this study, we interpreted transport phenomena near solid–liquid interfaces as successive hopping motions between adsorption layers (adsorption and desorption events) and expressed their frequency using rate constants. Furthermore, we developed a theoretical model to quantitatively predict these rate constants based on the Arrhenius equation and transition state theory (TST). To validate the constructed theoretical model, molecular dynamics (MD) simulations were performed for two representative systems: a simple model consisting of Pt as the solid wall and Ar as the liquid molecule, and a more realistic system with SiO_2 and H_2O. The results showed that the initial desorption from the adsorption layer can be well described by the theoretical model, whereas subsequent desorption proceeds more slowly than predicted. The observed discrepancy between the theoretical model and the simulations was attributed to the breakdown of the quasi-equilibrium assumption in TST for the molecules remaining in the adsorption layer. To interpret this mismatch, we proposed a conceptual model that focuses on molecular recrossing events at the adsorption-layer boundary. It is expected to provide useful guidance for future modeling of transport phenomena near solid surfaces.

I. INTRODUCTION

In recent years, semiconductor devices, as well as microelectromechanical systems (MEMS) and nanoelectromechanical systems (NEMS), have become essential components of everyday electronic equipment, playing a vital role in modern life. As these devices continue to evolve toward greater miniaturization and higher performance, there is an increasing demand for more advanced and precise fabrication technologies. One such crucial process in the manufacturing chain is the wet cleaning process. This process removes microscopic impurities and residues generated during fabrication, directly impacting device performance and production yield. With the ongoing miniaturization of device features to the nanoscale, a critical issue has emerged: the collapse of nanopatterns on silicon wafers during the drying step following cleaning. This collapse is known to result from the high surface tension of water, which is commonly used as the cleaning solvent.[1–4] To address this problem, a liquid displacement process using isopropyl alcohol (IPA), which has a lower surface tension than water, has been introduced. This process replaces water within the nanopatterns with IPA prior to drying.[5,6] Meanwhile, challenges such as residual water and re-adsorption of impurities remain in the IPA replacement process. Unfortunately, currently, this approach is based mostly on trial and error; thus, optimizing it requires a thorough understanding of mass transport properties within the confined regions of nanostructures.

For these reasons, it is important to clarify the transport phenomena of liquids near solid–liquid interfaces. However, experimental observations of such nanoscale phenomena are limited by

experimental conditions and the types of data that can be obtained. Therefore, molecular dynamics (MD) simulations, which allow phenomena to be captured on atomic and molecular spatiotemporal scales, are highly effective. Numerous studies have investigated the diffusion behavior of liquids near solid–liquid interfaces using MD simulations.[7,8] It has been shown that liquid molecules near such interfaces form stratified adsorption layers parallel to the surface. Regarding in-plane (parallel) transport phenomena, studies have commonly assumed uniform diffusion within these layers and have evaluated diffusion coefficients based on this assumption. Methods used include the Green–Kubo relation,[9,10] which relies on the velocity autocorrelation function, and the Einstein relation, based on the mean square displacement. For example, the previous study of our group computed diffusion coefficients for water and IPA molecules near SiO_2 walls, demonstrating that diffusion is slower in adsorption layers closer to the wall and approaches bulk values with increasing distance from the surface.[8]

In contrast, diffusion perpendicular to the solid–liquid interface exhibits anisotropic behavior due to the presence along the transport direction. This complexity renders conventional isotropic diffusion models inadequate. To capture this anisotropy, one promising approach involves using the Potential of Mean Force (PMF) distribution,[11] which quantifies a potential that provides the average force acting on a molecule and reflects the changes in free energy along the direction of interest.[12–16] The model represents molecular transport as a combination of a drift term, which depends on the gradient of the PMF, and random Brownian motion determined by the diffusion coefficient. A diffusion coefficient is sought such that the resulting transport behavior matches the actual observed transport. By examining the distance dependence of the obtained diffusion coefficient from the interface, the transport properties near the interface are quantitatively evaluated. While this model is suitable for the quantitative evaluation of transport properties, it is not appropriate for quantitative predictions.

As an alternative approach to the above model, our group previously proposed a model that treats transport in the direction normal to the interface as a series of jumping motions between adjacent adsorption layers.[17] We further attempted to describe this jumping motion by drawing an analogy to chemical reactions and applying the Arrhenius framework. In this framework, molecular transport is modeled as repeated adsorption to and desorption from discrete layers. The frequency of adsorption and desorption at each layer is described kinetically using rate constants. Thus, the overall transport characteristics could be quantitatively captured by the magnitude of these rate constants. Furthermore, the relationship between the free energy barrier that a molecule must overcome during desorption and the corresponding rate constant was also analyzed. This analysis was conducted using molecular dynamics simulations, focusing on the transport of Ar molecules near a Pt wall as a simplified model system. The logarithm of the rate constants exhibits a linear relationship with the free energy barriers, indicating that they follow the Arrhenius relation. This supports the usefulness of the model for describing transport properties in the direction normal to the interface. However, the system analyzed is highly simplified, and more general phenomena closer to real-world conditions have not yet been explored. In addition, a theoretical framework to predict the slope of the Arrhenius plot has not been established, leaving challenges for achieving quantitative predictive capability. Furthermore, while a good qualitative match was obtained, the Arrhenius relation did not necessarily hold quantitatively.

To address this, the present study aimed to develop a theoretical model capable of quantitatively predicting rate constants based on the Arrhenius equation. This was achieved by employing transition state theory (TST)[18] to compute the reaction rate factors from PMF distributions. The validity of the model was then examined by comparison with molecular dynamics simulation results. Two systems were considered: a simplified model using Pt as the solid wall and Ar as the liquid molecule, and a realistic system using SiO_2 and water. First, we analyzed the adsorption structures of the liquid molecules near the solid–liquid interface in both systems. Then, we evaluated the adsorption and desorption kinetics to extract rate constants, which were compared against the predictions of the proposed theoretical model based on TST. We critically examined the assumptions underlying TST, considering the observed discrepancies and identifying their limitations. Finally, by explicitly considering recrossing events, in which desorbed molecules rapidly return to the original or neighboring adsorption layer, we propose a conceptual model for guiding modifications to the theoretical model.

II. SIMULATION DETAILS

To analyze the behavior of the liquid molecules near the solid–liquid interface, molecular dynamics (MD) simulations were performed, where the liquid is confined between two parallel solid walls. Figures 1(a) and 1(b) show snapshots of the two systems analyzed in this study: the Pt–Ar system and the SiO_2–H_2O system, respectively. The coordinate system was defined such that the z-axis is perpendicular to the solid–liquid interface. Periodic boundary conditions were applied in the x and y directions.

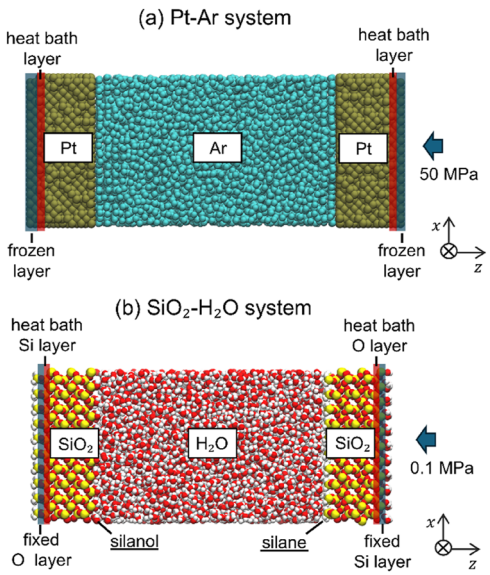

FIG. 1. Schematic of the simulation system that reproduces liquid confined by solid walls: (a) Pt–Ar system and (b) SiO_2–H_2O system.

For the Pt–Ar system, the potential model for Ar molecules was described using the Lennard–Jones (LJ) potential, expressed as follows:

$$U_{\mathrm{LJ}} = 4\varepsilon\left[\left(\frac{\sigma}{r}\right)^{12} - \left(\frac{\sigma}{r}\right)^{6}\right], \quad (1)$$

where the parameters were set to $\varepsilon = 0.238$ kcal/mol and $\sigma = 3.424$ Å.[19] The Pt walls were modeled using the Morse potential, expressed as follows:

$$U_{\mathrm{Morse}} = \mathrm{D}\left[e^{-2\alpha(r-r_o)} - e^{-\alpha(r-r_o)}\right], \quad (2)$$

where the parameters were set to $D = 2.39$ kcal/mol, $\alpha = 1.85$ Å^{-1}, and $r_0 = 2.77$ Å.[20] The interactions between Pt and Ar atoms were modeled using the LJ potential with $\varepsilon = 0.157$ kcal/mol and $\sigma = 3.424$ Å.[21] The cutoff radius for the LJ potential and Morse potential was set to be 12 Å. The Pt solid wall had an FCC crystal structure, and its (001) surface was in contact with the liquid. Under these parameters, the contact angle was found to be 41°, indicating good wettability. The wall dimensions were $5.87 \times 5.87 \times 2.744$ nm^3, consisting of $30 \times 30 \times 14$ atomic layers. The simulation system contained 6750 Ar molecules. The system was simulated under conditions of 100 K and 50 MPa so that argon remained in the liquid state.

For the SiO_2–H_2O system, the water molecules were modeled using the SPC/E model.[22] This model is known to reproduce the self-diffusion coefficient close to the experimental value under ambient temperature and pressure,[23] making it well suited for analysis of transport properties. As SPC/E is a rigid model, bond lengths and angles were constrained using the RATTLE algorithm.[24] The potential model for SiO_2 is based on the CHARMM force field.[25] In Ref. 25, this potential has been shown to reproduce experimentally observed trends in the dynamical behavior of confined water, including changes in translational and rotational dynamics. Therefore, this potential model is particularly suitable for investigating the transport properties of water molecules near SiO_2 solid walls in this study. Intermolecular interactions between SiO_2 and H_2O were described using the LJ and Coulomb potentials. The LJ parameters for SiO_2–H_2O interactions were determined using the Lorentz–Berthelot mixing rules. Long-range Coulomb interactions were computed using the particle–particle particle–mesh (PPPM) method,[26] with an accuracy of 10^{-4}. The crystalline structure of SiO_2 was set as α-quartz, the stable structure at ambient temperature and pressure, with the (001) surface in contact with liquid water. On the (001) surfaces, each Si atom possesses two dangling bonds, known as germinal. To remove these dangling bonds, the SiO_2 surfaces were terminated with silane (Si–H) on the right side of the wall and silanol (Si–OH) on the left side of the wall. The silanol-terminated surface exhibits complete wetting with water, whereas the silane-terminated surface shows a finite contact angle of 76.5°. The wettability analysis is based on the calculation of the work of adhesion using the phantom-wall method,[27–29] and the detailed procedure and results are provided in Sec. S1 of the supplementary material. The Si–H and O–H bond lengths in these terminal groups were also constrained using the RATTLE algorithm.[24] The wall dimensions were $4.32 \times 4.16 \times 1.84$ nm^3. The system contained 3680 H_2O molecules. The system was simulated at 300 K and 0.1 MPa. The cutoff distance is 12 Å for both LJ and Coulombic short-range interactions.

To achieve equilibrium at the target temperature and pressure, a relaxation run was first conducted. Pressure control was implemented by fixing the left wall's outermost layer and applying an external force to the right wall's outermost layer, as shown in Fig. 1. The thickness of the fixed layer was set to two Pt atomic layers in the Pt–Ar system, while in the SiO_2–H_2O system, it was set to one O atomic layer at the left wall and one Si atomic layer at the right wall. After performing at least 20 ns of simulation for system equilibration and confirming that the motion of the right wall had sufficiently converged, the position of the right wall's outermost layer was fixed at its equilibrium position. To complete the relaxation, an additional 1 ns of simulation was performed under these conditions. Following this, a production run of 20 ns was carried out to obtain data for analysis. Temperature control during both relaxation and production runs was performed by velocity scaling[30] of the atoms every 100 fs in the heat bath layers adjacent to the fixed layers, as shown in Fig. 1. The thickness of the heat bath was set to two Pt atomic layers in the Pt–Ar system, while in the SiO_2–H_2O system, it was set to one Si atomic layer at the left wall and one O atomic layer at the right wall. All simulations in this work were performed using a Large-scale Atomic/Molecular Massively Parallel Simulator (LAMMPS),[31] and we used Visual Molecular Dynamics (VMD)[32] software to visualize the molecular model construction.

III. RESULTS AND DISCUSSION

A. Adsorption structure of liquid molecules

In the simulated Pt–Ar and SiO_2–H_2O systems, we investigated the adsorption structures formed near the solid–liquid interfaces. Figures 2(a) and 2(b) show the number density distributions of argon molecules in the Pt–Ar system and water molecules in the SiO_2–H_2O system, respectively, along the direction normal to the interface (z-direction). In addition, for each system, the liquid density in the region sufficiently far from the solid surface, where the density becomes uniform, is also shown for reference. These distributions were calculated by averaging the number of molecules within rectangular slabs of 0.1 Å thickness along the z-axis. For water molecules, the distributions were obtained from the z-coordinate of their center of mass. The results reveal that several density peaks are observed near the interface, indicating the formation of layered adsorption structures, as has been widely reported in other studies. Furthermore, as shown in Fig. 2(b), it is observed that larger density peaks are present on the silanol side compared to the silane side, suggesting that silane groups absorb water molecules more strongly than silanol groups. In this study, each density peak was regarded as a distinct adsorption layer, and these layers were labeled as layer 1, layer 2, layer 3, and so on, with a larger number indicating being further from the wall side. Each adsorption layer was defined as the region between two adjacent local minima in the density profile. The density peaks of these adsorption layers gradually decreased with increasing distance from the interface, eventually approaching a uniform density in bulk regions sufficiently far from the wall. This is because the liquid molecules in layer 1 are trapped by the relatively stable potential of the solid wall, while those in the subsequent layers are influenced by the more fluctuating potential of the adjacent adsorption layers. For subsequent analysis, we considered five

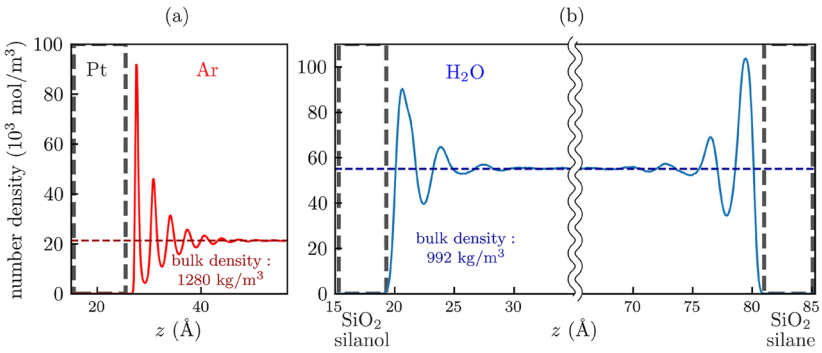

FIG. 2. Number density distributions of liquid molecules per area in the wall-normal direction: (a) Ar in the Pt–Ar system and (b) H_2O in the SiO_2–H_2O system.

adsorption layers formed on the solid–liquid interface in the Pt–Ar system, and three layers on each side in the SiO_2–H_2O system (six layers in total).

B. Arrhenius-based model of adsorption and desorption phenomena

Figure 3 illustrates the conceptual model for describing the transport behavior of liquid molecules in the direction normal to the solid–liquid interface used in this study. In this study, building upon our previous work,[17] we focus our analysis on the adsorption and desorption phenomena occurring between adjacent adsorption layers. As shown in Fig. 2, liquid molecules near the solid–liquid interface form structured adsorption layers. Molecules adsorbed within these layers can desorb by jumping to adjacent layers. Once desorbed, the molecules subsequently re-adsorb onto adjacent layers. The transport of liquid molecules in the interfacial region is thus governed by a series of discrete adsorption and desorption events. Consequently, the transport characteristics near the interface are governed by the frequency of these adsorption and desorption phenomena, rather than by continuous molecular diffusion, which is typically assumed in bulk phases. In this study, we quantitatively evaluated the adsorption and desorption phenomena by using rate constants that characterize the frequency of the desorption events. Furthermore, based on the Arrhenius equation, we constructed a theoretical model to predict these rate constants.

For molecules located in adsorption layer m at a given time, adsorption and desorption phenomena to the adjacent layers n and l are observed. Here, n, m, and l are consecutive natural numbers. The frequency of adsorption and desorption phenomena from layer m to its adjacent layers is quantitatively evaluated using rate constants, which are extracted from the simulation results as follows:

$$\frac{d(N_m(t))}{dt} = -k_m N_m(t), \tag{3}$$

$$\frac{d(N_{mn}(t))}{dt} = k_{mn} N_m(t), \tag{4}$$

$$\frac{d(N_{ml}(t))}{dt} = k_{ml} N_m(t), \tag{5}$$

$$k_m = k_{mn} + k_{ml}. \tag{6}$$

Here, N_m denotes the number of molecules that remained in layer m at time t without having crossed its boundaries since the initial observation. Here, the boundaries refer to the interfaces between adsorption layer m and its adjacent layers n and l, defined as the z-positions where the molecular density exhibits local minima. N_{mn} and N_{ml} represent the number of molecules that have desorbed and been adsorbed into layer n and layer l, respectively. In this study, a molecule is considered to have undergone adsorption and desorption phenomena if it crosses the boundary into an adjacent adsorption layer at least once. Recrossings, where a molecule returns to the original layer after crossing the boundary, are not taken into account during the counting, i.e., N never increases. This approach is adopted because the analysis focuses on the survival probability of the specific set of molecules adsorbed in the layer. By only tracking the set of molecules initially residing in the adsorption layer at the start of the observation, the lifetime of molecule adsorption can be determined. The parameters k_{mn} and k_{ml} in the equation are rate constants that characterize the adsorption and desorption dynamics toward layer n and layer l, respectively. The overall rate constant k_m represents the total rate of desorption events from layer m. Based on the definitions described above, the time evolution of the number of remaining and desorbed molecules was calculated for each adsorption layer using molecular trajectories obtained from the MD simulations.

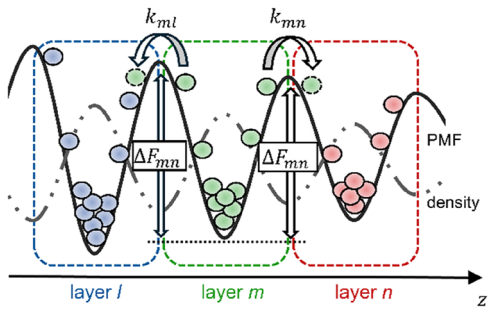

FIG. 3. Schematic illustration of adsorption and desorption phenomena from the adsorption layer m to the adjacent layers l and n.

Furthermore, to quantitatively predict the above rate constants from an alternative perspective, we described a theoretical model for adsorption and desorption phenomena based on the Arrhenius

equation. In a previous study by our group, theoretical models based on the Arrhenius equation were developed by focusing on the free energy barrier that liquid molecules must overcome when desorbing from an adsorption layer.[17] There, it was shown that the rate constants for adsorption and desorption are related to the free energy barrier through an Arrhenius-type relationship. In this study, we extended these existing models to construct an Arrhenius-based model capable of quantitatively predicting the rate constants.

The Arrhenius-based model focuses on the free energy barriers that molecules within an adsorption layer must overcome to desorb into the adjacent layers. As shown in Fig. 3, a molecule adsorbed in adsorption layer m must overcome a free energy barrier ΔF_{ml} to move to layer l and a barrier ΔF_{mn} to move to layer n. When a molecule desorbs from adsorption layer i to layer j, the rate constant k_{ij} for that process can be expressed, based on the Arrhenius equation, as follows:

$$k_{ij} = k_{i0} \exp\left(-\frac{\Delta F_{ij}}{k_B T}\right), \tag{7}$$

where k_B is the Boltzmann constant, T is the absolute temperature, and k_{i0} is the pre-exponential factor associated with layer i. The free energy barriers are determined from the potential of mean force (PMF) distribution corresponding to the adsorption layers. In the theoretical model, the reaction coordinate is defined along the z-axis; thus, we focus on the one-dimensional PMF profile in the z-direction. The PMF $F(z)$ as a function of position z, relative to the bulk region, can be related to the molecular number density distribution through the following equation:

$$F(z) = -k_B T \ln\left(\frac{\rho(z)}{\rho_0}\right), \tag{8}$$

where $F(z)$ is the free energy of a liquid molecule at position z relative to the bulk region, $\rho(z)$ is the number density at z, and ρ_0 is the number density in the bulk region. The magnitude of the free energy barrier that a molecule must overcome to move from adsorption layer i to layer j is given by

$$\Delta F_{ij} = -k_B T \ln\left(\frac{\rho_{\min}}{\rho_{\max}}\right), \tag{9}$$

where $\rho_{\max}$ is the maximum density within adsorption layer i and $\rho_{\min}$ is the minimum density at the boundary between layers i and j, corresponding to the lowest density along the path of transition. Furthermore, the pre-exponential factor associated with the process of a liquid molecule overcoming a one-dimensional energy barrier along the reaction coordinate can be calculated using transition state theory (TST)[18] as follows:

$$k_{i0}(T) = \frac{k_B T}{h Q^R(T)}, \tag{10}$$

$$Q^R = \sqrt{\frac{M k_B T}{2\pi h^2}} \int_{\text{well},i} \exp\left[-\frac{[F(z) - F_{\min}]}{k_B T}\right] dz, \tag{11}$$

where Q^R is the partition function of the reactant (the liquid molecules remaining within the adsorption layer), M is the mass of a liquid molecule, and h is Planck's constant. The integration range denoted as "well, i" corresponds to the entire region of adsorption layer i. Assuming the validity of the Arrhenius-based theoretical model described above, the adsorption and desorption rate constants can be expressed as

$$\frac{k_{ij}}{k_{i0}} = \frac{\rho_{\min}}{\rho_{\max}}. \tag{12}$$

The pre-exponential factor in this equation can be computed from the number density distribution using TST. Therefore, this model demonstrates that the rate constant governing the kinetics of adsorption and desorption phenomena can be predicted solely based on the density distribution, which is a static property.

C. Analysis of the applicability of Arrhenius-based model

To evaluate the validity of the Arrhenius-based model developed in Sec. III B, we compared the theoretical rate constants obtained from the model with the observed rate constants derived from actual adsorption and desorption phenomena captured in the simulations. The analysis was performed for all ten adsorption layers in the Pt–Ar system and all six layers in the SiO_2–H_2O system, as introduced in Sec. III A.

We tracked the time evolution of the number of remaining and desorbed molecules for each adsorption layer. The molecule counts were determined by checking every 50 fs whether each molecule had desorbed from the adsorption layer or remained within it. This interval of 50 fs was selected to reduce data size while still providing sufficient temporal resolution to resolve adsorption and desorption events. In addition, the analysis was repeatedly performed by changing the initial time step by 50 fs. For each initial time step $t_1, t_2, \ldots$, the survival probability of molecules present in the adsorption layer was evaluated independently, and the resulting survival probabilities were then averaged to obtain the statistical quantities. By averaging the survival probabilities with different time origins in this manner, sufficient statistical accuracy was maintained at each time even as the total number of molecules remaining in the adsorption layer decreased over time. The left panels of Fig. 4 show the analysis results of adsorption and desorption phenomena for layer 3 in the Pt–Ar system and layer 2 (silanol side) in the SiO_2–H_2O system, respectively, obtained from the MD trajectories. The number of desorbed molecules increases as the number of remaining molecules decreases.

The rate constants were calculated based on the observed time evolution of the number of remaining and desorbed molecules. The observed rate constants were calculated at each time step by numerically differentiating the molecular counts using the following equation, with a time interval of $\Delta t = 50$ fs:

$$k_{ij}(t) = \frac{N_{ij}(t + \Delta t) - N_{ij}(t)}{N_i(t)\Delta t}. \tag{13}$$

Although the theoretical model assumes constant rate constants, we deliberately examined their time dependence to more rigorously assess the model's validity. The right panels of Fig. 4 show comparisons between the rate constants obtained from adsorption and desorption phenomena observed in the MD simulations and those predicted by the Arrhenius-based model. The error bands

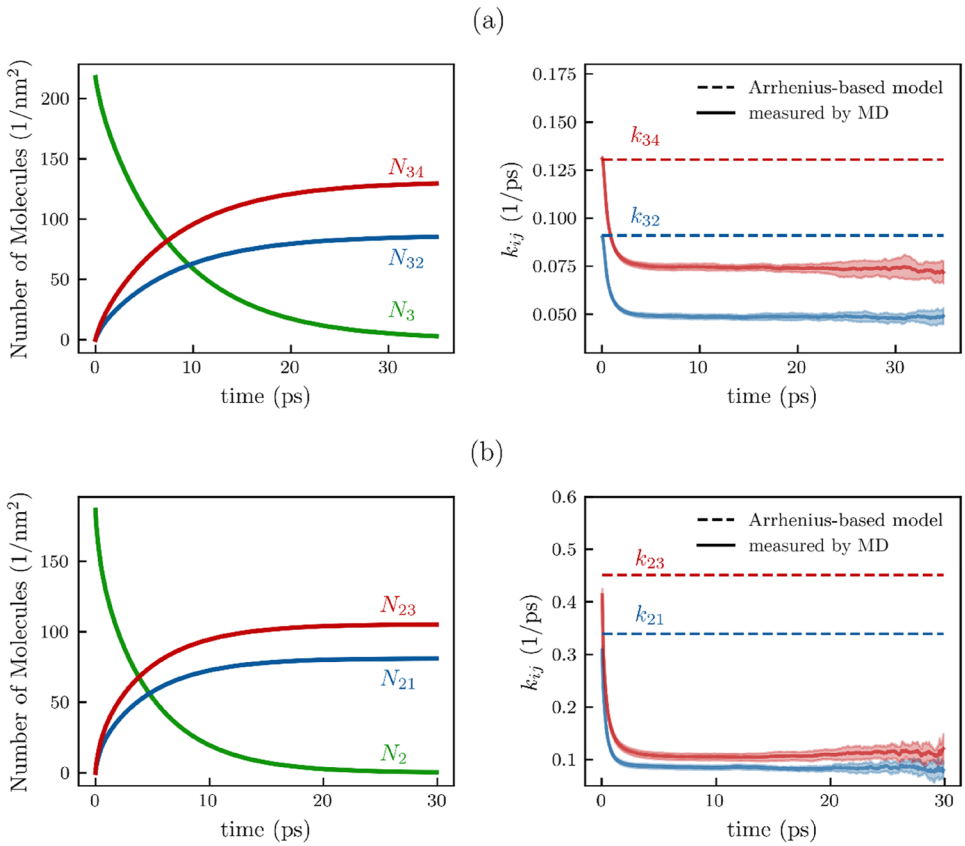

FIG. 4. Left panels: Time evolution of the number of molecules that remain within a given adsorption layer, N_i, and those that have desorbed, N_{ij}. Right panels: Comparison of the time evolution of the rate constants measured from MD simulations and those predicted by the Arrhenius model. [(a) and (b)] Results for layer 3 in the Pt–Ar system and layer 2 in the SiO_2–H_2O system (silanol side), respectively.

in the figure were calculated by dividing the 10 ns trajectory into 1 ns blocks to account for statistical inefficiency.[33] In both cases, the observed values reached a maximum at the initial time and then decayed to a steady-state value. These observed values generally agreed with the theoretical predictions at the initial stage. This trend was consistently observed across all adsorption layers.

Figure 5(a) also shows the comparison of the theoretical and observed rate constants at the initial time for all adsorption layers. Each observed initial rate constant $k(0)$ is plotted against the corresponding theoretical prediction based on Eq. (12). The dashed line in the figure represents the values predicted by the Arrhenius-based model described by Eq. (12). The error bars were calculated using the same method as in Fig. 4(b), taking statistical inefficiency into account.[32] The data points of the initial rate constant $k(0)$ closely follow the theoretical line, indicating that the Arrhenius-based model effectively describes the initial adsorption and desorption kinetics. Figure 5(b) presents a comparison between the converged values of the observed rate constants and the corresponding theoretical values. The converged values were defined as the first values at which the rate constant showed a change of less than 1% over a 0.5 ps interval. The error bars were calculated using the same method, as shown in Fig. 5(b). The observed values exhibit proportional relationships between ρ_{min}/ρ_{max} and k_{ij}/k_{i0}, with system-dependent differences in their slopes. The proportional relationship suggests that the model captures the qualitative trend, namely a linear correlation between ρ_{min}/ρ_{max}, which is related to the potential barrier height, and the normalized rate constant k_{ij}/k_{i0}, implying that an Arrhenius-type dependence is qualitatively maintained. However, the observed values are consistently lower than the theoretical ones, indicating that the model cannot quantitatively predict the long-time behavior.

In summary, the Arrhenius-based model accurately describes the initial adsorption and desorption kinetics, but its ability to predict long-time behavior remains limited. The actual process appears to follow a two-stage mechanism: an initial rapid desorption phase followed by a slower steady-state phase. The rate constants at the initial time are related to the number of molecules crossing the boundary of the adsorption layer in the equilibrium distribution. Meanwhile, the slower steady-state phase corresponds to the rate constants for desorption of molecules that have been adsorbed on the layer for a longer time. Evaluating the adsorption and desorption of these strongly adsorbed molecules is critically important for accurately characterizing the overall transport phenomena. Accurately predicting the rate constants in the latter regime remains a subject for future investigation.

D. Analysis of distributional changes beyond TST assumptions

To analyze the difference between the observed and theoretical values found in Sec. III C, we focus on the assumptions made in Transition State Theory (TST). First, we briefly outline a simple

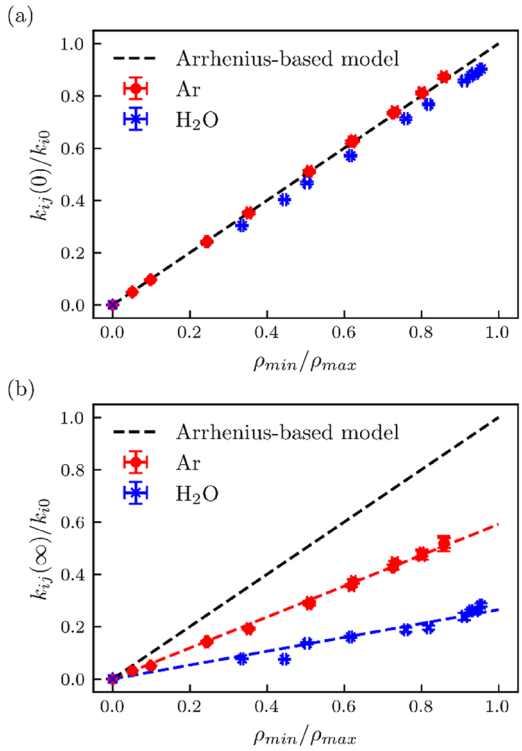

FIG. 5. Comparison between the rate constant calculated from the theoretical model and (a) the initial values and (b) the converged values of the rate constant, measured from MD simulations.

derivation of TST. The rate constant for desorption from layer i to layer j represents the probability flux of remaining molecules moving to layer j. Therefore, the rate constant k_{ij} can be expressed as follows:

$$k_{ij}(t) = p_i\left(t, z_{\text{edge}}\right) v_i^{\text{out}}\left(t, z_{\text{edge}}\right), \tag{14}$$

$$\int_{i,\text{well}} p_i(t,z)dz = 1, \tag{15}$$

$$v_i^{\text{out}}\left(t, z_{\text{edge}}\right) = \begin{cases} \int_0^\infty v f_i\left(t, z_{\text{edge}}, v\right)dv & \text{if } z_{\text{edge}} \text{ is right side,} \\ \int_{-\infty}^0 -v f_i\left(t, z_{\text{edge}}, v\right)dv & \text{if } z_{\text{edge}} \text{ is left side,} \end{cases} \tag{16}$$

$$\int_{-\infty}^{\infty} f_i\left(t, z_{\text{edge}}, v\right)dv = 1, \tag{17}$$

where z_{edge} denotes the z-coordinate at the boundary between adsorption layers i and j. The function $p_i(t,z)$ represents the position probability distribution of the remaining molecules along the reaction coordinate z at time t, normalized over the entire adsorption layer, as indicated in Eq. (15). Thus, $p_i\left(t, z_{\text{edge}}\right)$ gives the probability that a remaining molecule is located at the boundary between layers i and j at time t. The function $v_i^{\text{out}}\left(t, z_{\text{edge}}\right)$ denotes the average velocity of those molecules at the reaction edge that possess velocity components directed toward desorption, as described in Eq. (16). The function $f_i(t,z\ ,v)$ represents the velocity probability distribution of the remaining molecules at position z, and as shown in Eq. (17), it is normalized. In Eq. (16), molecules that do not move in the desorption direction are not included in the integration range, since they do not contribute to desorption. In the case of the Boltzmann distribution, for example, half of the molecules located at the adsorption layer boundary have velocity components directed toward the desorption direction, while the other half move in the opposite direction and thus do not contribute to desorption. In this case, $v_i^{\text{out}}\left(t, z_{\text{edge}}\right)$ corresponds to half of the mean speed of the full distribution. TST assumes that the position and velocity probability distributions of reactants (remaining molecules) remain unchanged even as the reaction (desorption) proceeds; this is referred to as the quasi-equilibrium assumption.[18] Moreover, it is assumed that these probability distributions coincide with the Boltzmann distribution. Based on these assumptions, Eq. (14) can be developed into Eq. (12).

We examined whether these assumptions are valid in the context of actual adsorption and desorption phenomena. To assess the validity of these assumptions in actual adsorption–desorption phenomena, we first examined the validity of the assumption that the position probability distribution $p_i(t,z)$ remains static, i.e., the supposition that the probability distribution function of molecules remaining in the adsorption layer is time invariant. Thus, the distribution of molecules remaining within a given adsorption layer was calculated at different time steps. To ensure statistical reliability, the analysis was performed in the same manner as the counting of remaining molecules described in Sec. III C: the time evolution of the spatial distribution of remaining molecules was calculated using multiple distinct time origins over a total duration of 20 ns, and the resulting distributions were averaged. The left panels of Figs. 6(a) and 6(b) show the time evolution of these distributions for adsorption layer 3 in the Pt–Ar system and layer 2 in the SiO_2–H_2O system (silanol side), respectively. The spatial distributions of the remaining molecules shown in the figure are normalized according to Eq. (15). We refer to z_{left} and z_{right} as the z-coordinates at the left and right boundaries of the adsorption layer, respectively. While the initial distributions agreed well with the equilibrium distribution, a time-dependent shift was observed as the number of remaining molecules decreased. In particular, molecules tended to cluster toward the center of the adsorption layer, and the density near the edges of the layer declined. This indicates a breakdown of the static distribution assumption of TST. Under equilibrium conditions, the stationary distribution is maintained by a balance between molecular outflux and influx across the layer boundaries. In the present analysis, however, the distributions were constructed solely from molecules that had never left the adsorption layer from the start of observation, and molecules entering the layer from neighboring regions were intentionally excluded. Therefore, the compensating influx required to sustain the equilibrium distribution at the boundaries is absent. This leads to an effective erosion of the distribution near the layer edges, resulting in a steady-state distribution that is biased toward the interior of the layer. The right panels of Figs. 6(a) and 6(b) represent the time evolution of the edge probability: $p_i\left(t, z_{\text{edge}}\right)$. The error bands in the figure were estimated by dividing the 20 ns trajectory into 2 ns blocks in order to account for statistical inefficiency.[33]

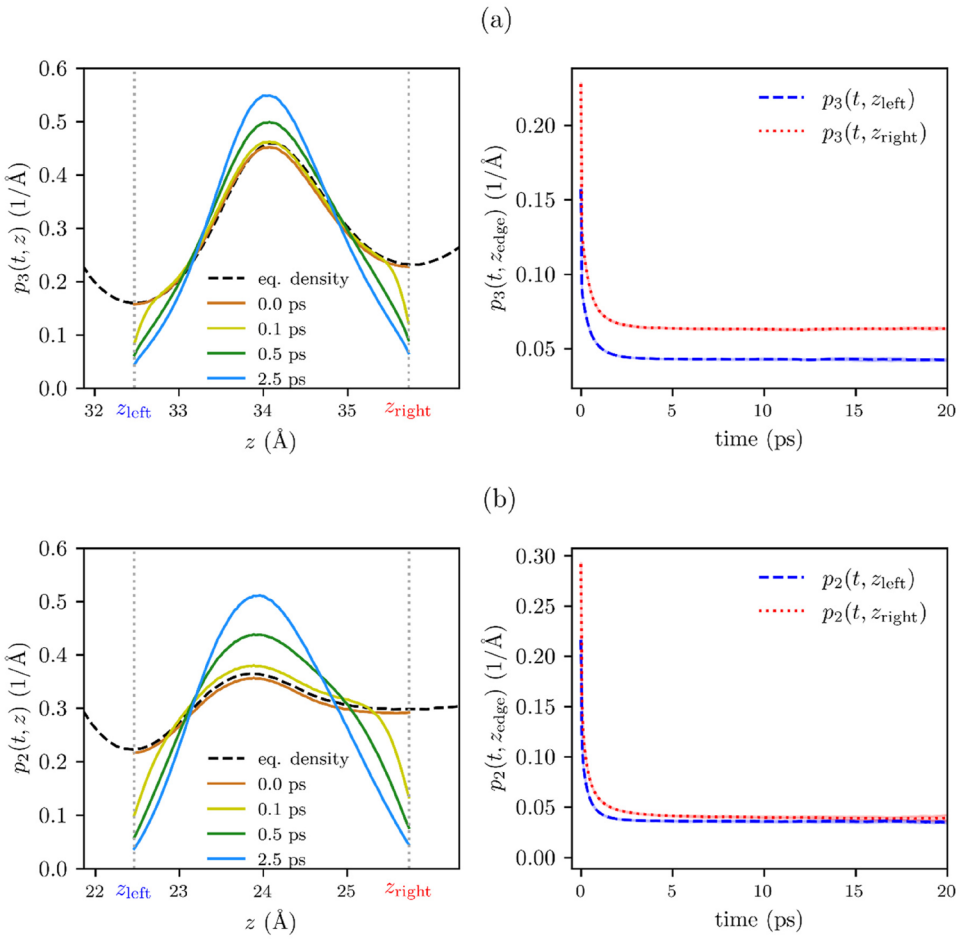

FIG. 6. Left panel: Time evolution of the position distributions of molecules remaining in an adsorption layer. Right panels: Time evolution of the edge probability. [(a) and (b)] Results for layer 3 in the Pt–Ar system and layer 2 in the SiO_2–H_2O system (silanol side), respectively.

The values of $p_i(t, z_{\mathrm{edge}})$ showed a rapid decrease from the initial value, followed by convergence to a lower steady-state value. This behavior closely matches the observed decay in the rate constants. As shown in Eq. (14), the rate constant is proportional to $p_i(t, z_{\mathrm{edge}})$. Therefore, the decrease in the edge probability can be considered a contributing factor to the reduction in the observed rate constants of adsorption and desorption phenomena. More detailed analysis of the time evolution of $p_i(t, z_{\mathrm{edge}})$ and the adsorption-layer dependence of its converged value is provided in Sec. S2 of the supplementary material.

Next, we evaluated the assumption concerning the velocity distribution $v_i^{\mathrm{out}}(t, z_{\mathrm{edge}})$. In transition state theory (TST), it is assumed that the velocity distribution of the remaining molecules does not deviate from the Maxwell distribution over time. To examine the validity of this assumption, we analyzed the time evolution of the velocity distribution of the remaining molecules located at the boundary of the adsorption layer. The calculation was performed by defining a probe volume with a thickness of 0.1 Å in the z-direction, located just inside the boundary of the adsorption layer. At each time point, the velocities of molecules present within this probe volume were collected for analysis. The thickness of 0.1 Å was chosen as a balance between sufficient resolution for capturing the velocities of molecules near the boundary and the computational cost of the analysis. As in the spatial distribution analysis, the time evolution of velocity distributions was evaluated using multiple time origins over a 20 ns trajectory and averaged to improve statistical accuracy. The left panels of Fig. 7 show the velocity distributions at the layer boundaries for the Pt–Ar and SiO_2–H_2O systems, respectively. The velocity distributions of the remaining molecules shown in the figure were normalized according to Eq. (17) at each time point. Initially, the distributions were consistent with the Maxwell distribution. However, as time progressed, the distributions shifted toward directions favorable for desorption, indicating a breakdown of the Maxwell distribution assumption of TST. Similarly to the spatial distributions, the velocity distributions deviate from equilibrium because only molecules remaining in the adsorption layer are considered, while inflowing molecules are excluded. As a result, the balance that sustains the Maxwell distribution is broken, leading to a nonequilibrium steady distribution biased toward desorption-favorable velocities. The right panels of Fig. 7 show the time evolution of the average velocity of desorbing molecules: $v_i^{\mathrm{out}}(t, z_{\mathrm{edge}})$. The error bands in the figure were estimated by dividing the 20 ns trajectory into 2 ns blocks to account for statistical inefficiency.[33] The average velocity starts from a minimum value at

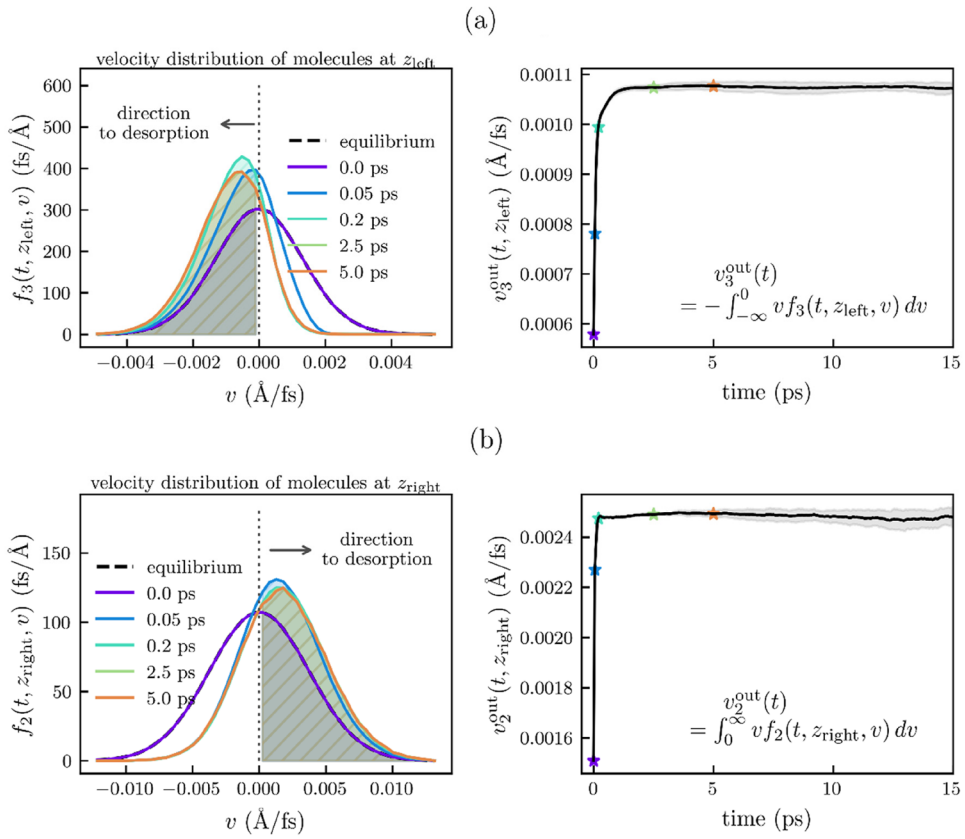

FIG. 7. Left panels: Time evolution of the velocity distribution of the remaining molecules located at the boundary of the adsorption layer. Right panels: Time evolution of $v_i^{\mathrm{out}}(t, z_{\mathrm{edge}})$ obtained from the velocity distribution. Here, $v_i^{\mathrm{out}}(t, z_{\mathrm{edge}})$ represents the average velocity of molecules moving in the desorption direction. The asterisks in the figure correspond to the colors used in the left panel, indicating the values at the respective time points represented by each color. [(a) and (b)] Results for the left side edge (z_{left}) of layer 3 in the Pt–Ar system and the right side edge (z_{right}) of layer 2 in the SiO_2–H_2O system (silanol side), respectively.

the initial time and gradually increases, eventually converging to a steady value. As indicated by Eq. (14), the rate constant is proportional to this average velocity. Therefore, the change in the velocity distribution of the remaining molecules acts to increase the rate constant over time. A more detailed analysis of the time dependence of $v_i^{\mathrm{out}}(t, z_{\mathrm{edge}})$ and the adsorption-layer dependence of its converged value of $v_i^{\mathrm{out}}(t, z_{\mathrm{edge}})$ is provided in Sec. S2 of the supplementary material.

These comparisons between TST assumptions and the observed adsorption and desorption behavior explain the decay in the observed rate constants. At initial times, as shown in Figs. 4 and 5(a), the theoretical and observed rate constants were in close agreement. This is because the initial distribution of the remaining molecules is the same as at the equilibrium state. However, as time progresses, the spatial and velocity distributions of the remaining molecules deviate from the equilibrium distribution, leading to discrepancies from the values of the Arrhenius-based model. Instead of maintaining equilibrium distributions, the remaining molecules evolve toward a new, steady-state distribution specific to the desorption process. The positional distribution shifts in a direction unfavorable for desorption, while the velocity distribution shifts in a direction favorable for it. These changes in the distributions explain the observed time dependence of the rate constants, which eventually converge to steady values. From the observed time evolution of the rate constants, positional distributions, and velocity distributions, it is suggested that the remaining molecules can be classified into two groups. One group exhibits a fast rate constant, predominantly observed near the initial observation time, corresponding to molecules that readily migrate out of the adsorption layer. The other group is characterized by a slower rate constant $k_{ij}(\infty)$ that dominates at later times. The equilibrium distribution can be regarded as the sum of the distributions associated with these two groups. As time progresses, molecules in the former group rapidly desorb from the layer. Consequently, the remaining population becomes increasingly dominated by molecules in the latter group, and the observed positional and velocity distributions gradually converge to those characteristics of this slower group. In Secs. III E and III F, we focus on recrossing events of these two groups of remaining molecules to further elucidate the underlying mechanism.

E. Effect of recrossing on the rate constant

Here, we interpret the fast desorption observed around the initial observation time in Sec. III C and the subsequent slow desorption characterized by the converged rate constant $k_{ij}(\infty)$ from the viewpoint of molecular recrossing. In this study, recrossing refers to a process in which a molecule that has desorbed once from an adsorption layer i into a neighboring layer j returns to the original layer i within a short time, without becoming sufficiently trapped in layer j. Because such interlayer motion occurs while the molecule is not yet strongly constrained in an adsorbed state, it is expected to be observed as a fast transport process. In this section, we quantitatively analyze the extent to which interlayer transport induced

by recrossing contributes to the rate constants. In particular, the molecules remaining in each adsorption layer at an early observation time were classified into two groups: molecules that had newly entered from a neighboring adsorption layer within 2 ps prior to the observation time, denoted as N_i^{new}, and molecules that had continuously resided in the same adsorption layer for longer than 2 ps, denoted as N_i^{old}. Accordingly, $N_i^{\mathrm{new}}(t) + N_i^{\mathrm{old}}(t)$ represents the total number of remaining molecules in the adsorption layer. The threshold of 2 ps was chosen based on the representative timescale at which the decay of the rate constant was observed in Sec. III C. For each of these two groups, the time evolution of the number of remaining molecules and the number of desorbed molecules was calculated. Using these time-dependent quantities, the contributions to the rate constant were then evaluated separately according to the following equations:

$$k_{ij}^{\mathrm{new}}(t) = \frac{1}{N_i^{\mathrm{new}}(t) + N_i^{\mathrm{old}}(t)} \frac{\left(N_{ij}^{\mathrm{new}}(t+\Delta t) - N_{ij}^{\mathrm{new}}(t)\right)}{\Delta t}, \quad (18)$$

$$k_{ij}^{\mathrm{old}}(t) = \frac{1}{N_i^{\mathrm{new}}(t) + N_i^{\mathrm{old}}(t)} \frac{\left(N_{ij}^{\mathrm{old}}(t+\Delta t) - N_{ij}^{\mathrm{old}}(t)\right)}{\Delta t}. \quad (19)$$

Here, the superscripts "new" and "old" attached to the remaining molecule numbers, the numbers of desorbed molecules, and the rate constants denote the contributions from molecules that migrated from a neighboring adsorption layer within the preceding 2 ps and from molecules that have remained in the same adsorption layer for longer than 2 ps, respectively. Figure 8 shows the time evolution of the rate constants decomposed according to Eqs. (18) and (19). Panel (a) presents k_{12} in the Pt–Ar system, while panel (b) shows k_{21} in the SiO_2–H_2O system. As shown in the figure, the large rate constants observed near the initial observation time are mainly due to the contribution from molecules that have recently entered from neighboring adsorption layers. This contribution corresponds to recrossing events, in which molecules that have once migrated into an adjacent adsorption layer return to the original layer on a short timescale. In other words, the fast interlayer transport observed around the initial time can be interpreted as a fast desorption process arising from molecular recrossing. These results indicate that, to quantitatively predict the rate constants for interlayer transport, it is essential to consider the fast interlayer motion induced by recrossing and the slower interlayer transport associated with molecules that are sufficiently adsorbed.

F. Conceptual transport model accounting for boundary recrossing events

Here, we discuss a conceptual model for devising modifications to the theoretical model, motivated by the relationship between recrossing events and the converged values of rate constants obtained in Sec. III C. As described in Sec. III E, migration accompanied by recrossing is a major factor responsible for the large rate constants observed near the initial time. Furthermore, the converged positional and velocity distributions of the remaining molecules shown in Sec. III D can be interpreted as the distribution of a molecular sub-ensemble consisting of molecules that have not undergone repeated recrossing up to that time. Accordingly, boundary-crossing events of the remaining molecules can be classified into two distinct processes: a fast process in which molecules rapidly cross back and forth across the layer boundary multiple times, and a comparatively slow process that proceeds without recrossing. In this section, these two transport processes are modeled according to the schematic pathway illustrated in Fig. 9. As depicted in Fig. 9, crossings at the layer boundary are decomposed into two contributions: direct crossings of the remaining molecules characterized by the rate constant $k_{ij}(\infty)$ and repeated boundary crossings occurring on an average of N_{cross} times. Here, recrossing is interpreted as multiple successive crossings of the layer boundary and is quantified by the number of such crossings. Once a molecule crosses the layer boundary in accordance with $k_{ij}(\infty)$, it is assumed to undergo, on average, N_{cross} boundary crossings before being re-adsorbed onto either of the adjacent adsorption layers. Thereafter, the molecule is assumed to re-enter the slow process governed by $k_{ij}(\infty)$, and this sequence is repeated. The initial crossing associated with $k_{ij}(\infty)$ is included in the definition of the average recrossing number N_{cross}, i.e., even if there is no recrossing $N_{\mathrm{cross}} = 1$. In the transport model, for simplicity, the left and right adjacent adsorption layers are assumed to be symmetric and to exhibit identical desorption behavior. Accordingly, attention is focused on the number of boundary-crossings per

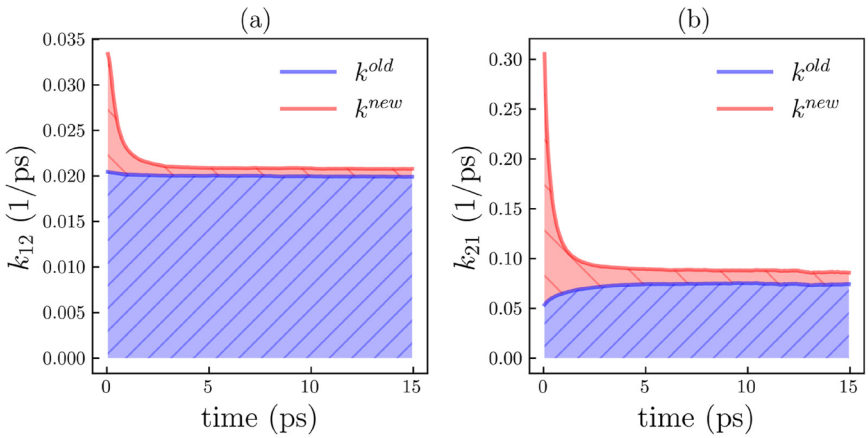

FIG. 8. Time evolution of the rate constants obtained from MD simulations, decomposed into contributions from molecules that entered the adsorption layer within the preceding 2 ps, k_{ij}^{new} (red), and from molecules that have continuously remained in the layer for longer than 2 ps, k_{ij}^{old} (blue): (a) k_{12} in the Pt–Ar system and (b) k_{21} in the SiO_2–H_2O system.

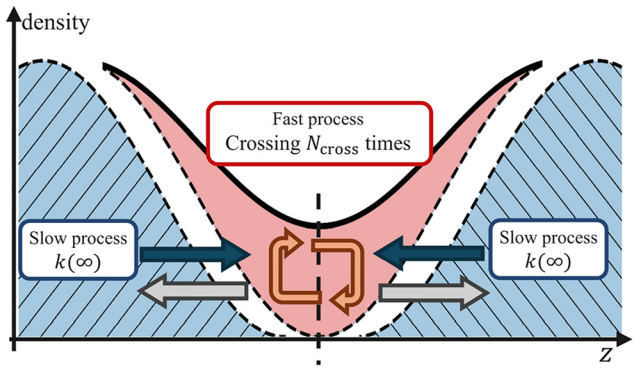

FIG. 9. Schematic illustration of the conceptual transport model based on the crossing number N_{cross}. Interlayer molecular transport is decomposed into a slow process governed by $k(\infty)$ and a fast process involving N_{cross} crossings at the layer boundary.

unit time in the positive and negative directions at the layer boundary. Under these assumptions, the following expression holds for the number of molecules crossing the layer boundary per unit time in equilibrium:

$$2k_{TST}N = 2N_{cross}k(\infty)N, \tag{20}$$

$$k(\infty) = \frac{k_{TST}}{N_{cross}}. \tag{21}$$

Here, N denotes the total number of remaining molecules, and k_{TST} is the rate constant obtained from Eq. (12). Within the model of transition state theory (TST), the rate constant k_{TST} is defined on the basis of the molecular flux across the layer boundary under the assumption of an equilibrium distribution. Accordingly, $k_{TST}N$ represents the number of molecules crossing the layer boundary per unit time in either positive or negative direction. Consequently, the total number of boundary-crossing events per unit time, summed over both directions, is given by $2k_{TST}N$. In the transport modeling proposed here, boundary crossing is initiated by a slow process characterized by the rate constant $k(\infty)$. For each such slow process, it is assumed that the molecule undergoes, on average, N_{cross} consecutive boundary crossings, including recrossing events. Under this assumption, the number of hopping events occurring per unit time is $k(\infty)N$, and each event gives rise to N_{cross} boundary crossings. Therefore, the total number of boundary-crossing events per unit time, including both directions, is expressed as $2N_{cross}k(\infty)N$. From Eq. (21), it follows that the converged value of the rate constant can be quantitatively related to the average number of recrossings at the layer boundary, N_{cross}. In this sense, Eq. (21) and the present model based on N_{cross} offer a physical interpretation of the difference between k_{TST} and $k(\infty)$, highlighting the role of recrossing processes in reducing the effective rate constant.

N_{cross} is defined as the mean number of times a molecule that has entered the vicinity of the layer boundary from either the left or the right adsorption layer via the rate $k_{ij}(\infty)$ subsequently undergoes repeated crossings of the boundary region. The present model does not provide a fully established quantitative scheme for predicting N_{cross}. As a possible approach to estimating this quantity, we, therefore, consider a stochastic description of boundary-crossing events based on Rice theory,[34,35] which enables the evaluation of level-crossing frequencies in random processes. In this Rice-theory-based evaluation, the recrossing problem at the layer boundary is reformulated as a problem of counting the number of crossings of the origin $z = 0$ by a particle that diffuses from the origin with a self-diffusion coefficient D_z at temperature T. According to Rice theory, the average number of crossings per unit time $\mu(t)$ of the reference position $z = 0$ at time t is given by

$$\mu(t) = \int_{-\infty}^{\infty} |v| p(z = 0, v, t)\ dv, \tag{22}$$

where $p(z = 0, v, t)$ represents the joint probability distribution of position and velocity at $z = 0$. The absolute value in Eq. (22) ensures that crossings in both the positive and negative directions are counted equally as single crossing events. In the present study, we assume that the molecular motion under consideration is in equilibrium and that the statistical properties of position and velocity are independent. Under this assumption, the joint distribution can be factorized as

$$p(z, v, t) = p(z, t)p(v), \tag{23}$$

where $p(z, t)$ and $p(v)$ represent the positional and velocity distributions, respectively. The positional distribution $p(z, t)$ is given by the solution of a one-dimensional diffusion process with a self-diffusion coefficient in the z direction, denoted by D_z, corresponding to particles initially localized at $z = 0$ at $t = 0$,

$$p(z, t) = \frac{1}{\sqrt{4\pi D_z t}} \exp\left(-\frac{z^2}{4D_z t}\right). \tag{24}$$

The velocity distribution $p(v)$ follows the equilibrium Maxwell distribution at temperature T and is expressed as follows, where m is the molecular mass:

$$p(v) = \sqrt{\frac{m}{2\pi k_B T}}\ \exp\left(-\frac{mv^2}{2k_B T}\right). \tag{25}$$

Substituting Eqs. (23)–(25) into Eq. (22), the crossing rate $\mu(t)$ can be written as

$$\mu(t) = \frac{1}{\pi}\sqrt{\frac{k_B T}{2mD_z t}}. \tag{26}$$

The cumulative number of crossings up to time t, denoted by $N_{cross}(t)$, is then obtained by integrating $\mu(t)$ over time,

$$N_{cross}(t) = \int_0^t \mu(t')dt' = \frac{2}{\pi}\sqrt{\frac{k_B T t}{2mD_z}}. \tag{27}$$

These expressions indicate that N_{cross} can be quantitatively evaluated from known physical parameters, such as temperature, molecular mass, and the self-diffusion coefficient. By substituting the resulting N_{cross} into Eq. (21), the converged value of the rate constant, $k(\infty)$, can be predicted within the present theoretical model.

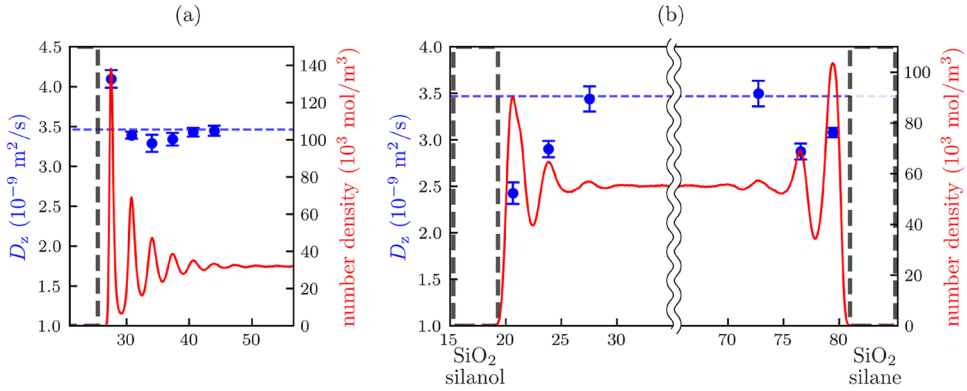

FIG. 10. Self-diffusion coefficients in each adsorption layer (blue) and number density distributions (red) of liquid molecules. The blue markers represent the self-diffusion coefficients in each adsorption layer, while the blue dashed line indicates the self-diffusion coefficient in the bulk region. Panel (a) shows the results for Ar molecules in the Pt–Ar system, and panel (b) shows those for H_2O molecules in the SiO_2–H_2O system.

In this study, the self-diffusion coefficients of liquid molecules appearing in Eq. (27) were evaluated separately for each adsorption layer. In the vicinity of the solid–liquid interface, molecular motion in the direction normal to the interface is strongly constrained by the adsorption, making it difficult to estimate the self-diffusion coefficient using the same methods as those applied to bulk liquids. Following previous studies,[12–16] the molecular motion normal to the interface was approximated as Brownian motion in an external field defined by the potential of mean force (PMF), and the self-diffusion coefficient was evaluated using the Langevin equation. Details of the computational procedure are provided in Sec. S3 of the supplementary material. The self-diffusion coefficients obtained by this method for liquid molecules in each adsorption layer of the Pt–Ar and SiO_2–H_2O systems are shown in Figs. 10(a) and 10(b), respectively.

Using the self-diffusion coefficients obtained for each adsorption layer, the converged values predicted by the conceptual model were evaluated by substituting them into Eqs. (21) and (27). However, when the recrossing number N_{cross} is evaluated using Eq. (27), $N_{\mathrm{cross}}(t)$ increases monotonically with time and does not exhibit a converged value. As a result, the time t remains as a fitting parameter in the evaluation of N_{cross}, which constitutes a limitation of the present Rice-theory-based formulation. To address this issue, we first examined at which time t produces N_{cross}, where Eq. (21) holds. Using a least-squares fitting procedure, we determined that Eq. (21) is satisfied on average at $t = 2.4$ ps for the Pt–Ar system, while for the SiO_2–H_2O system, it holds at $t = 1.7$ ps across all adsorption layers. Notably, this fitted timescale closely coincides with the timescale over which the rate constants obtained from the MD simulations converge to their steady values, as indicated in Fig. 4. In particular, the rate constants reach 95% of their converged value $k(\infty)$ after 2.34 ± 0.16 ps in the Pt–Ar system and 1.66 ± 0.18 ps in the SiO_2–H_2O system, where the uncertainties represent the variation among different adsorption layers. Both the absolute values and the relative ordering of these timescales are in good agreement with the fitted times. This correspondence provides physical justification for the choice of the fitting parameter and supports the validity of the proposed model, in which the rate constants are corrected based on the average recrossing number evaluated using Rice theory. By substituting these values of t yields, the recrossing numbers averaged over the different adsorption layers are obtained as $N_{\mathrm{cross}}(2.4\ \mathrm{ps}) = 1.7$ for the Pt–Ar system and $N_{\mathrm{cross}}(1.7\ \mathrm{ps}) = 3.9$ for the SiO_2–H_2O system. Using these representative times, the predicted rate constants were calculated and compared with the rate constants directly obtained from MD simulations, as shown in Fig. 11. As can be seen from the figure, good agreement is observed for all adsorption layers, demonstrating that the proposed model incorporating recrossing events is effective in quantitatively predicting the converged values of the rate constants. These results indicate that the present modeling, which focuses on molecular recrossing at layer boundaries, provides a useful model for describing transport phenomena between adsorption layers. Although the model still faces limitations in achieving fully quantitative predictions, it offers a physically transparent basis for understanding the role of recrossing events. In particular, the current formulation considers recrossing processes only on one side of an adsorption layer, and further refinement will require accounting for recrossing on both sides as well as the collective molecular dynamics within the entire adsorption layer. Addressing these issues is expected to lead to a more comprehensive and predictive theoretical model in future studies.

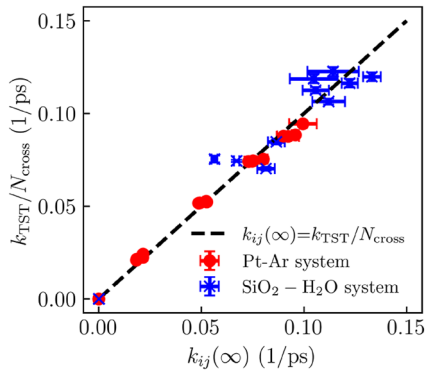

FIG. 11. Comparison between the converged rate constants $k_{ij}(\infty)$ obtained from MD simulations and those predicted by the conceptual model based on N_{cross}, as evaluated using Rice theory.

IV. CONCLUSION

In this study, we investigated the transport characteristics of liquid molecules in the direction normal to the solid–liquid

interface. Building upon previous research, the movement of liquid was modeled as a series of jumping events (adsorption and desorption phenomena) between discrete adsorption layers, and the frequency of these events was evaluated using kinetic analysis. Furthermore, a theoretical model was developed to quantitatively predict the corresponding rate constants based on transition state theory (TST).

We validated the theoretical model by comparing it with actual adsorption and desorption behavior observed in MD simulations. Two systems, the Pt–Ar system and the SiO_2–H_2O system, were examined. In both systems, liquid molecules near the interface formed multiple distinct adsorption layers. For each adsorption layer, we observed molecule migration during MD simulation. Across all systems and adsorption layers, the rate constants were found to be highest at the initial time and then decreased, eventually converging to a unique steady value for each layer and liquid type. Comparison with theoretical predictions showed excellent agreement at the initial stage. However, the steady state rate constants tended to be consistently lower than the theoretical ones by a constant factor. This indicates that while the theoretical model captures the qualitative features of the adsorption and desorption phenomena, it falls short in quantitatively describing the time-dependent behavior of the rate constants.

This discrepancy with the theoretical model was attributed to the breakdown of the quasi-equilibrium assumption in TST. In terms of positional distribution, molecules gradually concentrated near the center of the adsorption layer over time. As for the velocity distribution, it shifted in the direction of desorption. These changes in distributions are likely responsible for the observed deviations in rate constant from theoretical values. These results demonstrate the limitations of theoretical models based on TST.

Finally, by focusing on the number of molecular recrossing events at the adsorption layer boundary, we proposed a conceptual model that provides an interpretation for the discrepancies between the transport phenomena observed in MD and the theoretical model based on TST. This model explains the observed converged values of the rate constants by highlighting the role of recrossing processes in reducing the effective rate constant. Within this model, the observed transport behavior can be explained by considering that, on average, 1.7 recrossing events occur at the adsorption-layer boundary in the Pt–Ar system and 3.9 in the SiO_2–H_2O system. In addition, as a method for evaluating and predicting the number of recrossing events, we examined an approach based on Rice theory, which treats the frequency of reference-level crossings in stochastic processes. Although predictions of the converged rate constants based on this evaluation still face challenges in achieving fully quantitative accuracy, the approach was shown to capture the essential features of desorption dynamics between adsorption layers. The proposed model is, therefore, expected to provide useful guidance for future modeling of transport properties near solid surfaces. With further refinement of the modified model, improvements in the efficiency of wet processes, such as semiconductor cleaning and etching, are anticipated.

SUPPLEMENTARY MATERIAL

See the supplementary material for detailed descriptions of (i) the calculation of the contact angle of water on SiO_2 surfaces presented in Sec. II, (ii) the time evolution of the positional and velocity distributions of the remaining molecules discussed in Sec. III D, and (iii) the evaluation of the self-diffusion coefficient using the Langevin equation described in Sec. III F.

ACKNOWLEDGMENTS

Numerical simulations were performed on the supercomputer system "AFI-NITY II" at the Advanced Fluid Information Research Center, Institute of Fluid Science, Tohoku University.

AUTHOR DECLARATIONS

Conflict of Interest

The authors have no conflicts to disclose.

Author Contributions

Naohiro Dezawa: Conceptualization (equal); Data curation (equal); Formal analysis (equal); Methodology (equal); Software (equal); Visualization (equal); Writing – original draft (equal). **Donatas Surblys**: Conceptualization (equal); Methodology (equal); Project administration (equal); Software (equal); Supervision (equal); Writing – review & editing (equal). **Gota Kikugawa**: Conceptualization (equal); Methodology (equal); Project administration (equal); Writing – review & editing (equal). **Takeo Nakano**: Conceptualization (equal); Methodology (equal); Project administration (equal); Writing – review & editing (equal). **Taku Ohara**: Conceptualization (equal); Methodology (equal); Project administration (equal); Resources (equal); Supervision (equal); Writing – review & editing (equal).

DATA AVAILABILITY

The data that support the findings of this study are available from the corresponding author upon reasonable request.

REFERENCES

[1] H. Namatsu, M. Nagase, K. Kurihara, K. Iwadate, T. Furuta, and K. Murase, "Fabrication of sub-10-nm silicon lines with minimum fluctuation," J. Vac. Sci. Technol., B: Microelectron. Nanometer Struct. Process., Meas., Phenom. **13**(4), 1473–1476 (1995).

[2] D. S. L. Mui, N. Musselwhite, and M. Kawaguchi, "Factors influencing drying induced pattern collapse," Solid State Phenom. **282**, 201–206 (2018).

[3] T. Ghosh, E. C. Fritz, D. Balakrishnan, Z. Zhang, N. Vrancken, U. Anand, H. Zhang, N. D. Loh, X. Xu, F. Holsteyns, C. A. Nijhuis, and U. Mirsaidov, "Preventing the capillary-induced collapse of vertical nanostructures," ACS Appl. Mater. Interfaces **14**(4), 5537–5544 (2022).

[4] A. Hadjittofis, J. R. Lister, K. Singh, and D. Vella, "Evaporation effects in elastocapillary aggregation," J. Fluid Mech. **792**, 168–185 (2016).

[5] J. Koo, T. Kim, C. Jung, J. Lee, and T. Kim, "Effects of water and iso-propyl alcohol relative humidities on single wafer cleaning system performance," Int. J. Heat Mass Transfer **50**(21–22), 4275–4285 (2007).

[6] D. Eom, K. Kim, and Y. Shin, "Drying performance of single IPA dryer to prevent pattern collapse and watermark," ECS Trans. **41**(5), 197–204 (2011).

[7] P. Geysermans, D. Gorse, and V. Pontikis, "Molecular dynamics study of the solid–liquid interface," J. Chem. Phys. **113**(15), 6382–6389 (2000).

[8]Y. Naruke, S. Kosaka, T. Nakano, G. Kikugawa, and T. Ohara, "A molecular dynamics study on mass transport characteristics in the vicinity of SiO_2–water/IPA interfaces," Int. J. Heat Mass Transfer **84**, 584–591 (2015).
[9]R. Kubo, "Statistical Mechanical theory of irreversible processes. I. General theory and simple applications to magnetic and conduction problems," J. Phys. Soc. Jpn. **12**(6), 570–586 (1957).
[10]M. S. Green, "Markoff random processes and the statistical mechanics of time-dependent phenomena. II. Irreversible processes in fluids," J. Chem. Phys. **22**(3), 398–413 (1954).
[11]D. Frenkel and B. Smit, *Understanding Molecular Simulation: From Algorithms to Applications*, 3rd ed. (Elsevier B.V., Amsterdam, The Netherlands, 2023).
[12]K. Höllring, A. Baer, N. Vučemilović-Alagić, D. M. Smith, and A. S. Smith, "Anisotropic molecular diffusion in confinement I: Transport of small particles in potential and density gradients," J. Colloid Interface Sci. **650**, 1930–1940 (2023).
[13]P. Liu, E. Harder, and B. J. Berne, "On the calculation of diffusion coefficients in confined fluids and interfaces with an application to the liquid-vapor interface of water," J. Phys. Chem. B **108**(21), 6595–6602 (2004).
[14]P. J. Colmenares, F. López, and W. Olivares-Rivas, "Molecular dynamics and analytical Langevin equation approach for the self-diffusion constant of an anisotropic fluid," Phys. Rev. E **80**(6), 061123 (2009).
[15]W. Olivares-Rivas, P. J. Colmenares, and F. López, "Direct evaluation of the position dependent diffusion coefficient and persistence time from the equilibrium density profile in anisotropic fluids," J. Chem. Phys. **139**(7), 074103 (2013).
[16]C. D. Wick and L. X. Dang, "Diffusion at the liquid-vapor interface of an aqueous ionic solution utilizing a dual simulation technique," J. Phys. Chem. B **109**(32), 15574–15579 (2005).
[17]J. Suzuki, G. Kikugawa, T. Nakano, and T. Ohara, "Kinetic model for transport of liquid molecules in the solid-liquid interface region: A molecular dynamics view," Mech. Eng. Lett. **1**, 15-00353 (2015).
[18]J. I. Steinfeld, J. S. Francisco, and W. L. Hase, *Chemical Kinetics and Dynamics*, 2nd ed. (Prentice Hall, Upper Saddle River, New Jersey 07458, 1998).
[19]E. Ruckenstein and H. Liu, "Self-diffusion in gases and liquids," Ind. Eng. Chem. Res. **36**(9), 3927–3936 (1997).
[20]H. J. Castejón, "The effect of point defects on the scattering and trapping of rare gases on metallic surfaces," Surf. Sci. **564**(1–3), 165–172 (2004).
[21]P. Spijker, A. J. Markvoort, S. V. Nedea, and P. A. J. Hilbers, "Computation of accommodation coefficients and the use of velocity correlation profiles in molecular dynamics simulations," Phys. Rev. E **81**(1), 011203 (2010).
[22]H. J. C. Berendsen, J. R. Grigera, and T. P. Straatsma, "The missing term in effective pair potentials," J. Phys. Chem. **91**(24), 6269–6271 (1987).
[23]P. Mark and L. Nilsson, "Structure and dynamics of the TIP3P, SPC, and SPC/E water models at 298 K," J. Phys. Chem. A **105**(43), 9954–9960 (2001).
[24]H. C. Andersen, "Rattle: A 'velocity' version of the shake algorithm for molecular dynamics calculations," J. Comput. Phys. **52**(1), 24–34 (1983).
[25]P. E. M. Lopes, V. Murashov, M. Tazi, E. Demchuk, and A. D. MacKerell, "Development of an empirical force field for silica. Application to the quartz-water interface," J. Phys. Chem. B **110**(6), 2782–2792 (2006).
[26]R. W. Hockney and J. W. Eastwood, *Computer Simulation Using Particles* (Adam Hilger, 1989).
[27]F. Leroy and F. Müller-Plathe, "Solid-liquid surface free energy of Lennard–Jones liquid on smooth and rough surfaces computed by molecular dynamics using the phantom-wall method," J. Chem. Phys. **133**(4), 044110 (2010).
[28]F. Leroy, D. J. V. A. Dos Santos, and F. Müller-Plathe, "Interfacial excess free energies of solid-liquid interfaces by molecular dynamics simulation and thermodynamic integration," Macromol. Rapid Commun. **30**(9–10), 864–870 (2009).
[29]C. Bistafa, D. Surblys, H. Kusudo, and Y. Yamaguchi, "Water on hydroxylated silica surfaces: Work of adhesion, interfacial entropy, and droplet wetting," J. Chem. Phys. **155**(6), 064703 (2021).
[30]L. V. Woodcock, "Isothermal molecular dynamics calculations for liquid salts," Chem. Phys. Lett. **10**(3), 257–261 (1971).
[31]A. P. Thompson, H. M. Aktulga, R. Berger, D. S. Bolintineanu, W. M. Brown, P. S. Crozier, P. J. in 't Veld, A. Kohlmeyer, S. G. Moore, T. D. Nguyen, R. Shan, M. J. Stevens, J. Tranchida, C. Trott, and S. J. Plimpton, "LAMMPS—A flexible simulation tool for particle-based materials modeling at the atomic, meso, and continuum scales," Comput. Phys. Commun. **271**, 108171 (2022).
[32]W. Humphrey, A. Dalke, and K. Schulten, "VMD: Visual molecular dynamics," J. Mol. Graphics **14**(1), 33–38 (1996).
[33]M. P. Allen and D. J. Tildesley, *Computer Simulation of Liquids* (Oxford University Press, Great Clarendon Street, Oxford, 2009).
[34]S. O. Rice, "Mathematical analysis of random noise," Bell System Technical Journal **23**(3), 282–332 (1944).
[35]I. Rychlik, "On some reliability applications of rice's formula for the intensity of level crossings," Extremes **3**(4), 331–348 (2000).